

Experimental Study of Extreme Responses of a Point Absorber Wave Energy Converter

J. Orszaghova¹, A. Rafiee², H. Wolgamot¹, S. Draper¹ and P. H. Taylor¹

¹Faculty of Engineering, Computing and Mathematics
The University of Western Australia, Crawley, Western Australia 6009, Australia

²Carnegie Wave Energy Limited
Fremantle, Western Australia 6160, Australia

Abstract

Understanding the dynamics of wave energy converters (WECs) under extreme wave conditions is crucial when designing for their survivability. Results are presented from an experimental campaign investigating extreme responses of a model-scale WEC, representative of a submerged buoy WEC called CETO being developed by Carnegie Wave Energy Limited (CWE). The response parameter of interest is the model power take-off (PTO) extension, which corresponds to the piston stroke within the hydraulic cylinder of the prototype PTO system. The experimentally derived response amplitude operator (RAO), together with higher order response corrections, are shown to be effective in prediction of the extreme responses and the design wave groups leading to these extremes.

Introduction

CWE carried out an extensive set of laboratory experiments at Plymouth University COAST laboratory. As part of the programme, the model CETO device was subjected to a number of severe sea states to study the WEC's response in extreme conditions. All wave conditions presented herein were long-crested propagating normally to the line of wavemakers.

The sixth generation of the CETO technology consists of a large disc-shaped submerged buoy, referred to as the buoyant actuator (BA). Under wave action, the buoy moves in heave, surge and sway (as well as pitch, roll and yaw; with the rotational motions not coupled to the PTO). The prototype hydraulic PTO system consists of a hydraulic cylinder/pump, which is attached to the bottom of the BA. The CETO device is connected to a foundation on the sea bed via a tether. In the laboratory experiments, a mechanical winch was used to represent the hydraulic PTO system (see Figure 1). The tension and the length of the rope were measured and controlled by the PTO unit. For the laboratory experiments analysed in this work, the simplified PTO force corresponded to a linear spring-damper system such that

$$F_{PTO} = C_{PTO} + K_{PTO}(L_{PTO} - L_{PTO}^0) + B_{PTO}L'_{PTO}, \quad (1)$$

where C_{PTO} is the buoyancy force, K_{PTO} is the spring coefficient, B_{PTO} is the damping coefficient, $L_{PTO} - L_{PTO}^0$ represents the PTO extension and L'_{PTO} represents the PTO velocity.

Under long-crested conditions, the PTO extension is related to the buoy motion such that

$$\begin{aligned} L_{PTO} - L_{PTO}^0 &= \sqrt{(L_{PTO}^0 + Z)^2 + X^2} - L_{PTO}^0 \\ &\approx Z + \frac{X^2}{2L_{PTO}^0} + \dots, \end{aligned} \quad (2)$$

where X and Z are the surge and heave motions, and 2D Taylor series has been used to derive the approximation. Therefore, at first order, the PTO force is linearly proportional to heave, but overall the PTO force is non-linearly related to the BA motion.

Additionally, in the experiments the PTO force was bounded as $0 \leq F_{PTO} \leq F_{max}$, where $F_{max} = 1250$ N was reached during all the extreme PTO extension events discussed below.

In this study, the PTO extension was the response variable of interest. It is representative of the piston stroke within the hydraulic cylinder of the prototype PTO system, and as such is a design parameter affecting the sizing of the PTO system to minimise the probability of the piston hitting the end stops of the cylinder.

The experiments were carried out at 1:20.8 scale. For the severe irregular sea state, the underlying spectrum was Pierson-Moskowitz with $H_{m0} = 0.38$ m and $T_p = 3.07$ s (full scale significant wave height of 7.9 m and peak period of 14 s). Time series of free surface elevation, buoy motion (in 6 degrees of freedom), PTO load and PTO extension were recorded synchronously.

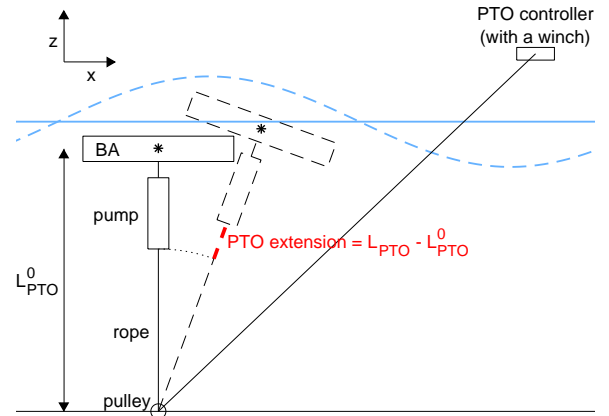


Figure 1: Schematic diagram of the model CETO device and the experimental PTO system.

Long duration irregular waves tests

The duration of the irregular tests was 2400 s, which corresponds to approximately 3 hours in full scale. Active absorption at the wavemaker and passive absorption at the far end of the basin were employed to minimise contamination by reflections. From the recorded PTO extension time series, the largest events were identified (see Figure 2a). The local time series were extracted for analysis which follows, and are plotted in Figure 2b with the peak PTO extensions aligned in time (here chosen to be $t = 0$ s). The free surface time series corresponding to the extracted PTO extension events are displayed in Figure 2c. Note that the free surface measurements were taken at a location which was the same distance from the wavemaker as the BA, but offset laterally to minimise the influence of the radiated and diffracted waves.

From the plots it follows that the maximum PTO extension events have locally very similar characteristics. The averaged shape of the maximum responses appears close to symmetric. The corresponding waves also exhibit similarities locally, suggesting that a particular wave group leads to the maximum PTO extension events. This localised wave shape comprises a deep trough just before the maximum PTO extension followed by a large crest just after the maximum PTO extension. This wave shape appears to be between a crest focused wave group and an up-crossing focused wave group.

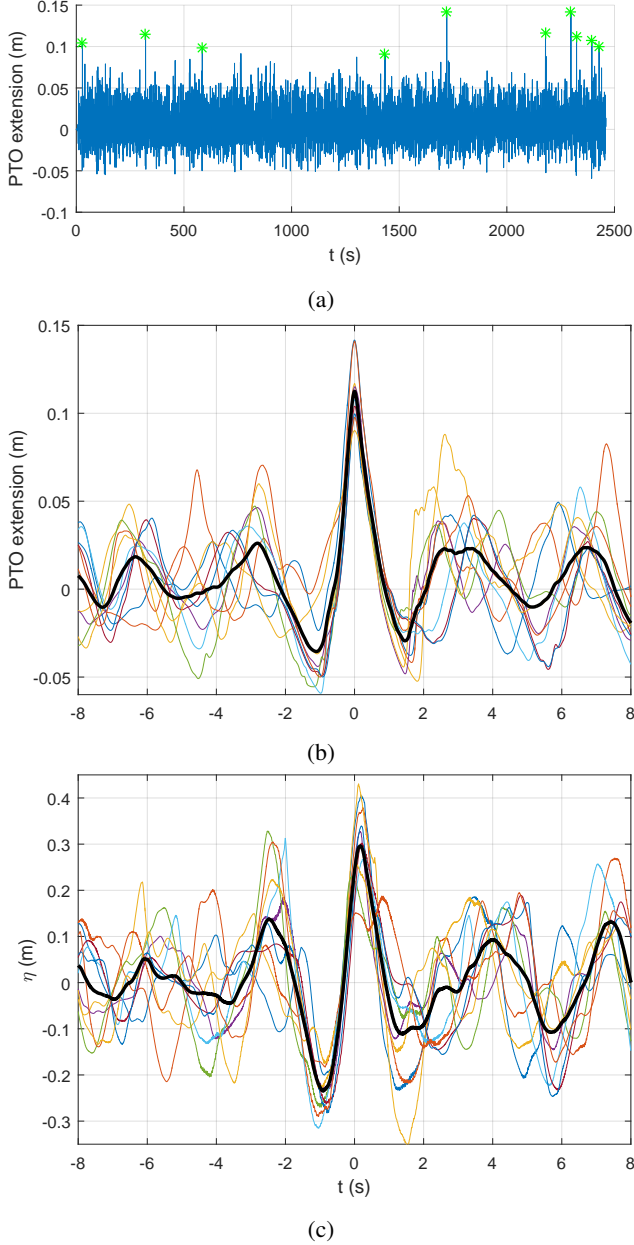


Figure 2: Irregular waves run. (a) PTO extension time series with the 10 maximum responses identified (green star markers). (b) Extracted maximum PTO extension events, together with the averaged shape (bold black line). (c) Free surface time series corresponding to the extracted maximum response events, together with the averaged shape (bold black line).

Short duration focused wave groups tests

A focused wave group comprises a number of harmonic compo-

nents which come in phase at one point in time and space. Due to the constructive interference between individual components, a focused wave group represents a large energetic compact wave event. Due to frequency dispersion, away from focus, the wave group is less compact and less violent. The linear free surface of a focused wave group is given by

$$\eta(x,t) = \sum_{i=1}^N a_i \cos(k_i(x-x_f) - \omega_i(t-t_f) - \phi_0), \quad (3)$$

where N is the total number of wave frequency components and a_i , k_i and ω_i are the amplitude, wave number and wave frequency of the i^{th} component. The phase of the wave group at focus (where $x = x_f$ and $t = t_f$) is denoted by ϕ_0 , with a crest focused wave group given by $\phi_0 = 0$ and an up-crossing focused wave group by $\phi_0 = -\pi/2$. According to NewWave theory (see [1], [2], [3]), the amplitude of each wave component follows directly from the underlying free surface variance density spectrum S such that

$$a_i = A \frac{S(\omega_i)\Delta\omega}{\sum_{j=1}^N S(\omega_j)\Delta\omega}, \quad (4)$$

where A is the target linear amplitude for a crest focused wave group. A crest focused NewWave represents the average shape of the largest wave in a linear Gaussian sea. Similarly, for a weakly non-linear response, a crest focused NewWave in response represents the average shape of the largest response (see [10] and [6]).

A focused wave group with $A = H_{m0}$ m and $\phi_0 = -\pi/3$ was generated in the basin. From Figure 3 it follows that the measured PTO extension is very similar to the largest PTO extension events from the irregular waves run, and as such this wave group could be a design wave for maximum PTO extension. It should be noted that under different wave conditions and different PTO settings, the design wave group could differ.

Separation of harmonics, RAO analysis and approximate higher order terms

Additionally, crest and trough focused wave group experiments were performed in the basin. Under the assumption that the free surface measurements and the response of interest possess a Stokes-like structure, separation of harmonics can be performed. Subtraction and addition of the crest and trough time series give the odd and even harmonic component time series respectively. With application of band-pass digital filters with appropriate cut-off frequencies, linear, second order super- and sub-harmonic and third order super-harmonic components can be separated (see for example [7]). It should be noted that harmonic decomposition utilising four phase-shifted focused wave group runs (see [4]) is preferable, but due to time constraints in the basin was not achievable. The harmonic structure of the PTO extension is shown in Figure 4. It is seen that the linear signal is dominant, with the second and third order responses being smaller, yet not insignificant. Corresponding plot of the harmonic decomposition of the free surface is omitted for brevity.

Using the linearised free surface and PTO extension, the linear transfer function, or the response amplitude operator (RAO), is derived. Figure 5 shows the RAO amplitude, as well as the RAO phase angle which gives the phase shift between the input free surface and the response PTO extension. Note that the RAO values displayed are the averaged values across the two focused wave tests and the irregular waves test, and that the RAO is approximate, since the system under consideration is not, in fact, linear. The RAO phase angle is around $\pi/3$ rad for the most

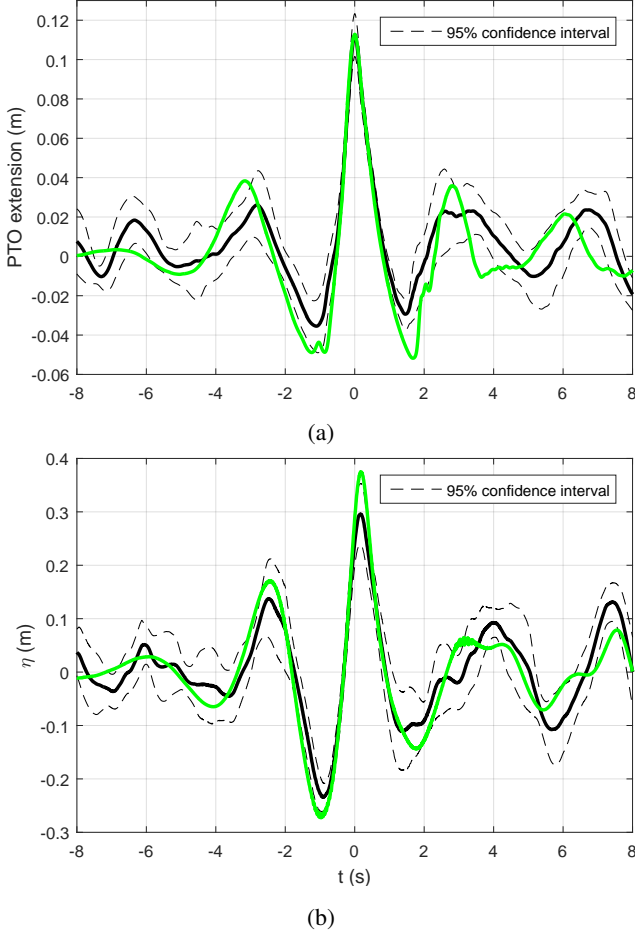


Figure 3: (a) PTO extension time series from the focused wave group run (bold green line) superimposed on the maximum averaged response events from the irregular waves run. (b) Focused wave group (bold green line) superimposed on the averaged free surface time series corresponding to the extracted maximum response events from the irregular waves run.

energetic part of the spectrum, which is consistent with our earlier finding that a $\phi_0 = -\pi/3$ focused wave group leads to the largest PTO extension response.

Next, we attempt to approximate the non-linear contributions to the free surface and the response using the linearised time series. Following [5] and [6], the second and third order corrections might be approximated by

$$\begin{aligned}
 y_{2-} &\approx B^- \left((y_1)^2 + (H[y_1])^2 \right), \\
 y_{2+} &\approx B_{in}^+ \left((y_1)^2 - (H[y_1])^2 \right) + B_{out}^+ 2 y_1 H[y_1], \\
 y_{3+} &\approx C_{in}^+ \left((y_1)^3 - 3 y_1 (H[y_1])^2 \right) + C_{out}^+ \left(3 H[y_1] (y_1)^2 - (H[y_1])^3 \right),
 \end{aligned} \tag{5}$$

where y_1 and $H[y_1]$ denote the linearised signal and its Hilbert transform, y_{2+} , y_{2-} and y_{3+} represent the second order super-, second order sub- and third order super-harmonic contributions. The scaling coefficients B^- , B_{in}^+ , B_{out}^+ , C_{in}^+ and C_{out}^+ need to be determined. The subscripts *in* and *out* refer to being in phase and being in quadrature ($\pi/2$ out of phase) with the linear components respectively. For super-harmonic bound waves, the out of phase terms are zero (i.e. $B_{out}^+ = C_{out}^+ = 0$). The above procedure works for a narrow-banded process, whereby the single values of the scaling coefficients provide an appropriate approximation of the interaction kernels, and where there is no dynamics in the

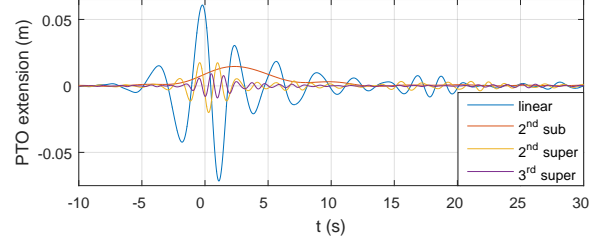


Figure 4: Harmonic structure of the measured PTO extension.

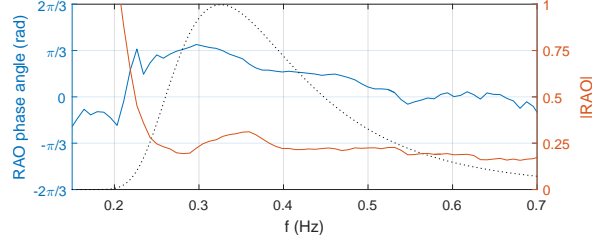


Figure 5: RAO amplitude (solid red line) and RAO phase angle (solid blue line) for PTO extension. For reference, the dotted line shows the spectral shape considered with $T_p = 3.07$ s.

response function.

Figure 6 shows comparison between the measured and the approximated higher order responses. The fitted second order scaling coefficients B^- , B_{in}^+ and B_{out}^+ were 2.7, 3.3 and -2.2m^{-1} , and the third order coefficient C_{in}^+ and C_{out}^+ were 11 and -22m^{-2} . This implies that phase shifts of 0.59 and 1.1 rad were applied to the super-harmonic PTO extension corrections. From the plots it follows that the second and third order PTO extension can be reasonably approximated using the linearised response signal. Note that the main group spans approximately $-5 \leq t \leq 5$ s. The measured responses beyond $t \approx 5$ s are due to incident error waves and backwards travelling reflected components. Corresponding comparison plots for free surface elevation are omitted for brevity, but we report that the approximation works very well for the bound wave prediction, as it should. The second and third order bound waves can also be calculated via the interaction kernels given by [8] and [9].

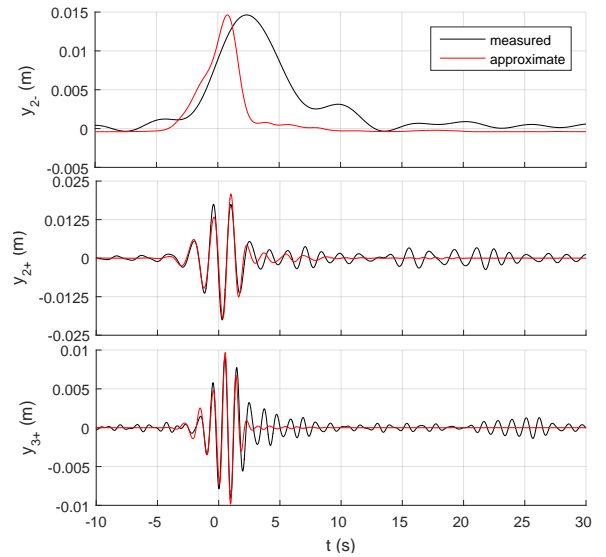


Figure 6: Approximations of the higher harmonic PTO extension based on the linearised response time series.

Extreme response prediction

We are now equipped to predict the largest (positive and negative) responses, as well as the responses due to the largest wave crests (or deepest troughs). Starting with the input wave spectrum, the response spectrum is calculated via the RAO. The largest positive (linear) response is then given by a superposition of all the response components with their crests aligned (NewWave in response). The corresponding (linear) free surface time series is calculated via the complex RAO applied to each component, such that both amplitude and phase are altered. The higher order responses, and bound waves, are estimated from the linear time series as explained above.

Figure 7a shows the predicted maximum PTO extension, with the peak value chosen to match the experiments. The predicted PTO extension time series gives a good approximation locally to the averaged largest responses from the irregular waves run. We note the importance of the second and third order corrections to the PTO extension. The predicted design wave shown in 7b is representative of the extracted waves from the irregular run. Note that the design wave is not a focused wave group. For the same level of peak response, the $\phi_0 = -\pi/3$ focused wave group is larger compared to the predicted design wave. This should not be surprising, as the design wave represents the least energetic wave group leading to the prescribed level of response as its frequency content is appropriately chosen to maximise the response under consideration (i.e. wave frequency components which do not excite the system are minimal).

Similarly, one can predict response due the largest wave (i.e. due to NewWave crest focused wave group). The resulting PTO extension is smaller. Therefore the largest waves do not lead to the largest response for the test case considered (this would apply for situations with very small RAO phase angles).

Conclusions

Analysis of maximum PTO extension for a model-scale WEC was performed. Prediction of a design wave group leading the largest response was demonstrated with the use of phase-shifted focused wave groups. For the wave conditions and the PTO settings considered, the predicted largest PTO extension and the corresponding design wave matched the extracted extremes from the irregular waves run. Due to the RAO phase angle being around $\pi/3$ rad over the energetic part of the underlying wave spectrum considered, the design wave was suitably approximated by a $\phi_0 = -\pi/3$ focused wave group.

Considering the non-linear characteristics of the PTO system and the fact that localised wave breaking occurred in the tests, the prediction method (which relies on Stokes expansion being valid) worked rather well in the case considered. Further analysis is needed under different PTO and wave conditions.

This research was supported under Australian Research Council's Linkage Projects funding scheme (LP150100598).

References

- [1] Tromans, P.S., Anaturk, A. R. and Hagemeyer, P., A new model for the kinematics of large ocean waves application as a design wave, Proc. of the First International Offshore and Polar Engineering Conf., 3, 64 - 71, 1991.
- [2] Lindgren, G., Some properties of a normal process near a local maximum, The Annals of Mathematical Statistics, 41, 1870 - 1883, 1970.
- [3] Boccotti, P., Some new results on statistical properties of wind waves, Applied Ocean Res., 5, 134 - 140, 1983.

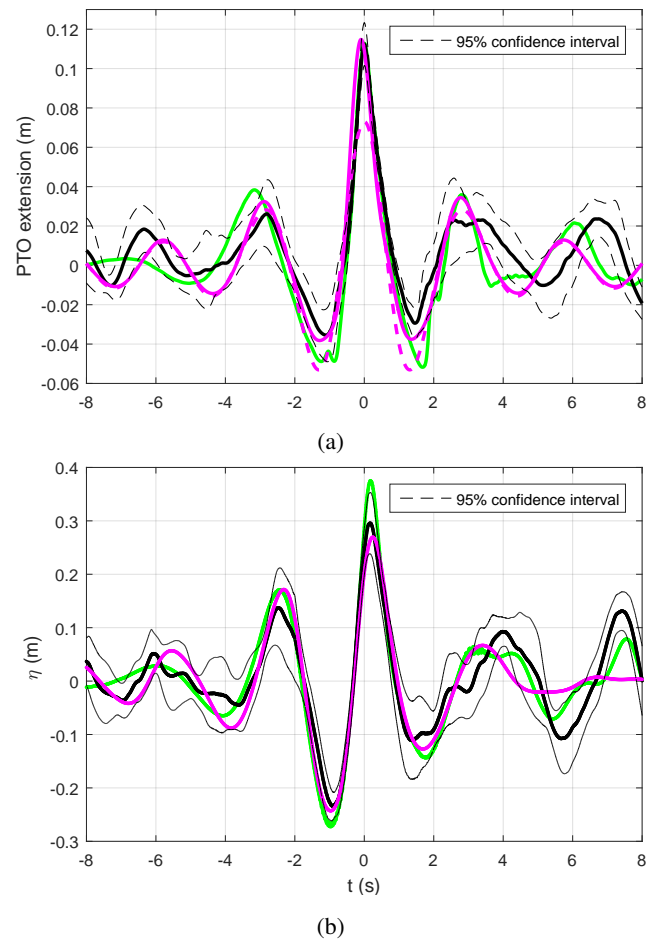


Figure 7: (a) Predicted linear (dashed pink line) and non-linear (solid pink line) maximum PTO extension time series. (b) Corresponding predicted design wave (solid pink line, including second order bound waves).

- [4] Fitzgerald, C.J., Taylor, P.H., Eatock Taylor, R., Grice, J. and Zang, J., Phase manipulation and the harmonic components of ringing forces on a surface-piercing column, Proc. R. Soc. A, 470, 2014.
- [5] Walker, D.A.G., Taylor, P.H. and Eatock Taylor, R., The shape of large surface waves on the open sea and the Draupner New Year wave, Applied Ocean Res., 26, 73 - 83, 2004.
- [6] Santo, H., Taylor, P.H., Moreno, E.C., Eatock Taylor, R., Stansby, P., Sun, L. and Zang, J., Extreme motion and response statistics for survival of the M4 wave energy converter, under consideration for Journal of Fluid Mechanics.
- [7] Orszaghova, J., Taylor, P.H., Borthwick, A.G.L. and Raby, A.C., Importance of second-order wave generation for focused wave group run-up and overtopping, Coastal Engineering, 94, 63 - 79, 2014.
- [8] Dalzell, J.F., A note on finite depth second-order wave-wave interactions, Applied Ocean Res., 21, 105 - 111, 1999.
- [9] Madsen, P.A. and Fuhrman D.R., Third-order theory for multi-directional irregular waves, Journal of Fluid Mechanics, 698, 304 - 334, 2012.
- [10] Grice, J.R., Taylor, P.H. and Eatock Taylor, R., Near-trapping effects for multi-column structures in deterministic and random waves, Ocean Engineering, 58, 60 - 77, 2013.